Atomic structure of chlorinated Si(113) surfaces

J. I. Flege,[1,2,*] Th. Schmidt,[2] M. Siebert,[2] G. Materlik,[3] and J. Falta[2]
[1]*Hamburger Synchrotronstrahlungslabor HASYLAB/DESY, Notkestrasse 85, 22603 Hamburg, Germany*
[2]*Institut für Festkörperphysik, Universität Bremen, Otto-Hahn-Allee 1, 28359 Bremen, Germany*
[3]*Diamond Light Source Limited, Diamond House, Chilton, Didcot, Oxfordshire OX11 0DE, United Kingdom*
(Received 27 September 2007; revised manuscript received 23 July 2008; published 21 August 2008)

We present a detailed investigation of the adsorption of Cl on the Si(113) surface based on x-ray standing-wave experiments and density-functional theory calculations with additional characterization by low-energy electron diffraction and scanning tunneling microscopy. For the whole accessible range of Cl coverages, $(2\times n)$-like surface reconstructions are identified. Despite this apparent complexity, it is shown that these surface structures consist of only a few atomic adsorption geometries with the most prominent one being the Cl adsorption on top of a Si surface adatom. The required redistribution of Si concurs with a pronounced straightening and alignment of step edges along the $[1\bar{1}0]$ direction. Furthermore, it is argued that this adatom site plays a key role in step-edge geometries on vicinal Si(111) and Si(001) surfaces.

DOI: 10.1103/PhysRevB.78.085317 PACS number(s): 68.49.Uv, 68.43.Fg, 68.43.Bc

I. INTRODUCTION

High-index silicon surfaces have attracted an increasing interest due to their possible application for nanostructuring. Specifically, for the Si(113) surface orientation, it has already been shown that high-quality surface oxides comparable to the one for the technologically established Si(001) surface[1] may be prepared. Furthermore, the absence of rotational symmetry may also be utilized for the growth of one-dimensional Ge nanowires[2–4] or controlled adsorbate-induced surface faceting.[5–7]

From a structural point of view, the Si(113) surface may be conceived as a mixture of atomic rows of Si(111)- and Si(001)-like atoms, or, equivalently, as maximally stepped Si(111) and Si(001) surfaces, respectively. While the clean Si(113) surface is thermodynamically stable against faceting and displays a (3×2) reconstruction[8,9] involving sixfold coordinated Si interstitial atoms,[10] these can be expected to be easily destabilized by adsorption of hydrogen[11] or, e.g., halogens. Hence, studying the interaction of halogens with the Si(113) surface may be a well-suited means to investigate faceting tendencies in the presence of adsorbates and to experimentally shed light on the corresponding step-edge structures.

So far, little attention has been paid to the interaction of the Si(113) surface with halogens, which are well known to play a crucial role in wet-chemical etching reactions[12] and semiconductor processing as well as for template creation in subsequent surface functionalization with organics. With respect to chemical applications, the bulk-terminated Si(113) surface exhibits two chemically different surface atoms per unit cell, i.e., one Si(001)-like atom with two dangling bonds and one Si(111)-like atom with a single unsaturated orbital. These sites may serve as effective reaction sites for selective surface chemistry, possibly facilitating the creation of atomically ordered one-dimensional templates for further processing.

Recently,[13] we reported on the variety of $(2\times n)$ surface reconstructions with $n=2,3,5,\ldots$ found by scanning tunneling microscopy (STM) of the Cl/Si(113) system, which coexist after exposure to Cl_2 at 600 °C. Moreover, it was demonstrated that all superstructures found may be decomposed into similar subunits irrespective of the specific value of n. In the present paper, we address the atomic structure within this "building block" by means of x-ray standing waves (XSW) and *ab initio* density-functional theory (DFT).

II. EXPERIMENT

The XSW experiments were performed at the Hamburg Synchrotron Radiation Laboratory (HASYLAB). Details of the ultrahigh-vacuum XSW setup located at the undulator beamline BW1 have been published elsewhere.[14] In a typical XSW measurement, the sample reflectivity and the yield of an inelastic (secondary) signal, i.e., here Cl 1*s* photoelectrons, are recorded while tuning the incident photon energy through the Bragg condition of the (*hkl*) diffraction planes of the substrate crystal. As monochromators, pairs of symmetrically and asymmetrically cut Si(111) and Si(220) crystals were employed. This setup allowed the nondispersive investigation of the (111) and the (022) Bragg reflections at a photon energy of 3.35 keV, i.e., in an energy regime well above the Cl *K* absorption edge at 2.82 keV. Additionally, XSW measurements were also conducted in dispersive [using the (220) monochromator crystal pair] and nondispersive (113) geometries at 3.93 keV to investigate the effect of dispersiveness on the data evaluation and structural modeling.

If the intensity of the detected secondary signal is proportional to the intensity of the x-ray interference field, then an analysis of the intensity modulation of the secondary signal according to the dynamical theory of x-ray diffraction[15] directly yields the modulus and phase of the (*hkl*) Fourier component of the spatial distribution function of the atoms contributing to the chosen signal.[16] These quantities are commonly denoted as *coherent fraction* f_c^{hkl} and *coherent position* Φ_c^{hkl}, respectively. The experimental errors for these parameters due to Poisson statistics and least-square fitting routines have been determined to be less than $\Delta f_c \lesssim 0.02$ and $\Delta\Phi_c \lesssim 0.01$ for all data sets presented in the following section. If photoelectrons are used as secondary signal, further

uncertainties generally arise from nondipole contributions. These multipole contributions can only be taken into account if additional parameters are introduced whose values cannot be determined experimentally in most cases and thus have to be derived theoretically.[17–20] For the present case of Cl 1*s* photoelectrons, a comparison with XSW data obtained by employing Cl K_α fluorescence yields almost identical coherent fractions and coherent positions, rendering nondipole contributions negligible at this photon energy.[14] However, with respect to the subsequent structural analysis using DFT, it should be kept in mind that, for complex adsorbate structures, additional sources of deviations occur, e.g., due to Gaussian error propagation in mixing atomic sites bearing individual uncertainties of a few hundredths of an Ångström with respect to the bulk reference position. For a more comprehensive discussion, the reader is referred to the literature.[14]

In the XSW experiments, RCA-cleaned[21] Si(113) substrates of 2 mm thickness were used. These samples were introduced into the UHV system and degassed for at least 12 h at 630 °C. Subsequent flashing to 880 °C for about 5 min removed the protective oxide layer and restored the (3×2) reconstruction[8,10] of the clean Si(113) surface, which was routinely monitored by low-energy electron diffraction (LEED). This procedure, i.e., using a thick substrate with a wet-chemically prepared thin oxide that can be removed at rather low temperatures, was employed in order to prevent thermally induced bending of the crystal, which would deteriorate the high bulk crystal quality necessary in the XSW experiments. With respect to the STM investigations, which were performed in a variable-temperature STM (Omicron), sample bending is not crucial. Therefore, commercial Si(113) wafers could be used and flashed to 1200 °C for a few seconds to create a clean (3×2) reconstructed surface. For both the XSW and the STM experiments, Cl deposition was achieved using a home-built AgCl electrochemical source[22] with the sample held at either room temperature (RT) or 600 °C. Additionally, the samples were annealed at elevated temperatures or evaporation times were reduced in order to prepare samples with a broad range of Cl coverages. For the XSW samples, the Cl coverages were calibrated by comparing the ratios of the Cl 1*s* and Si 1*s* photoemission intensities to the corresponding values obtained for the related system $Cl/Si(111)-(1\times1)$ at the same photon energy, and the same experimental geometry; the saturation coverage of which has been determined to be 1.0 ± 0.1 monolayers (ML) [1 $ML_{Si(111)}=7.84\times10^{14}$ atoms/cm^2].[23] In the following, the Cl coverages will be given in units of ML with respect to the Si(113) surface [1 $ML_{Si(113)}=4.09\times10^{14}$ atoms/cm^2].

III. RESULTS AND DISCUSSION

This section is organized as follows: In Sec. III A, we present LEED and STM results that serve to elucidate the long-range surface periodicity as well as the local atomic reconstruction. Further insight into the atomic structure is gained by detailed XSW investigations for samples with various Cl coverages, which are laid out in detail in Sec. III B. The inherent complexity of the emerging $(2\times n)$ surface unit cell is addressed with DFT calculations for atomic trial structures (Sec. III C). Fourier components are derived from these ground-state geometries and are then compared to the experimental XSW data, enabling a constrained search in developing a suitable structural model for the Cl/Si(113) system. Finally, the section closes with a discussion (Sec. III E) relating the obtained results to step-edge geometries found on Si(111) and vicinal Si(001) surfaces.

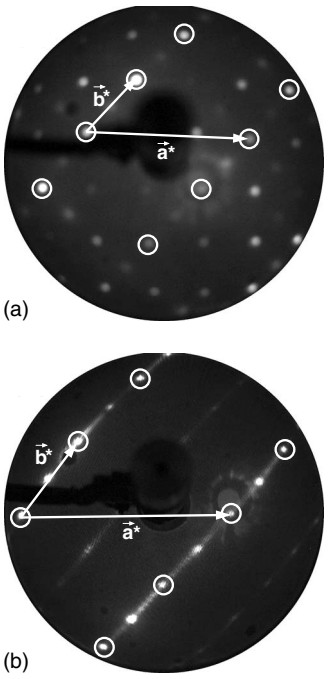

FIG. 1. (a) (3×2) LEED pattern ($E_{kin}=63$ eV) of the clean $Si(113)-(3\times2)$ surface and (b) $(2\times n)$ LEED pattern ($E_{kin}=60$ eV) of a Si(113) surface chlorinated at 600 °C, respectively. In both cases, the surface unit cells including the reciprocal-lattice vectors $\vec{a}^*$ and ($\vec{b}^*\|[33\bar{2}]$) are indicated.

A. Low-energy electron diffraction and scanning tunneling microscopy: surface reconstructions

For clarity, we will concentrate at first on the adsorption of Cl on the Si(113) surface at a sample temperature of 600 °C. In Fig. 1, LEED patterns of both the clean and the chlorinated Si(113) surface are supplied. The Cl deposit was determined to be 1.3 ± 0.2 ML after an exposure of Cl_2 equivalent to more than 100 ML at the sample position. As can be seen clearly, the initial (3×2) structure of the bare Si surface has vanished and a (2×2) periodicity with pronounced streaks in $\vec{b}^*$ direction appears. This is evidence for the rearrangement of surface atoms into a Cl-induced (2×2) reconstruction, very likely in coexistence with a variety of $(2\times n)$-like reconstructions similar to the case of Sb adsorption on Si(113).[24]

To investigate more closely the surface structure that leads to this complex LEED pattern, STM was performed on surfaces with similar coverages. The micrograph presented in Fig. 2 shows a chlorinated Si(113) surface after exposure to Cl_2 at 600 °C. As marked in the image, (2×3)-reconstructed

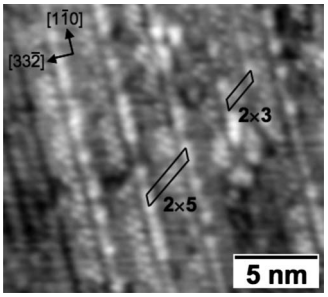

FIG. 2. STM image (U_{tip}=2.0 V, I=0.3 nA, and 20 nm ×20 nm) of the Si(113) surface after exposure to Cl_2 at 600 °C. A variety of $(2\times n)$-like surface reconstructions is observed. Exemplary surface unit cells are marked.

and (2×5)-reconstructed surface areas were observed along with a certain degree of disorder. Under these tunneling conditions, the surface unit cells are delimited by bright rows in [1$\bar{1}$0] direction with the space between them filled by densely packed chains of circular features. In connection with the (2×2) spots and the additional streaks found in the LEED investigation, these findings may be taken as evidence for the simultaneous occurrence of $(2\times n)$-like reconstructions with $n\in\{2,3,5,\ldots\}$. As the (2×3) and (2×5) reconstruction look somewhat similar in the STM images, it may already be argued at this early stage that the reconstructions should be made up of similar atomic subunits. This particular aspect is discussed in a separate publication[13] and strengthened by further evidence of (2×7)-reconstructed and (2×9)-periodic patches. However, in the following we will directly address the atomic structure of the Cl/Si(113)$-(2\times n)$ reconstruction with XSW and DFT.

B. X-ray standing waves: Atomic structure

The interpretation of a common atomic structure underlying the different reconstructions is endorsed by inspection of the XSW results (Fig. 3) for the sample whose LEED pattern is displayed in Fig. 1(b). For a mixture of substantially different surface reconstructions involving a fair number of inequivalent Cl adsorption sites, almost vanishing coherent fractions exhibiting values close to zero would be expected. However, the opposite is underlined by the relatively high coherent fractions of f^{113}=0.75 and f^{220}=0.77, which almost

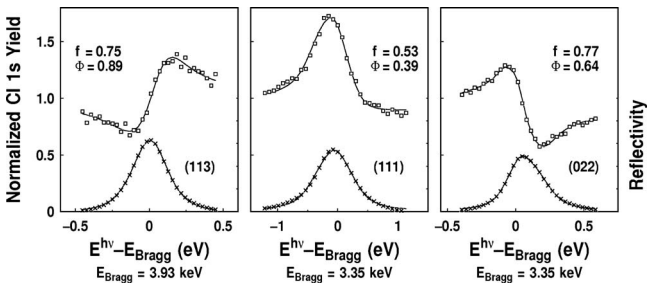

FIG. 3. XSW data and fit (solid lines) for sample reflectivity (×), and Cl 1s photoelectron yield (□) in (113), (111), and (022) Bragg reflections for Cl/Si(113)$-(2\times2)$ prepared at 600 °C. The Cl coverage amounts to approximately 1.3 $ML_{Si(113)}$.

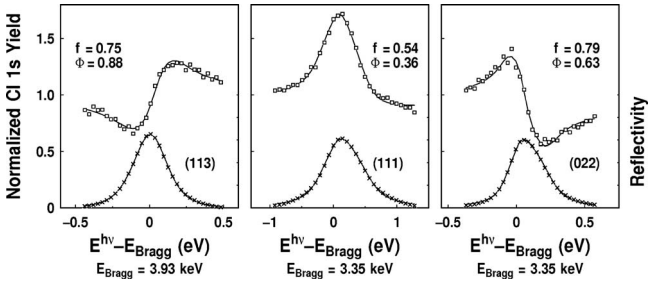

FIG. 4. XSW data and fit (solid lines) for sample reflectivity (×), and Cl 1s photoelectron yield (□) in (113), (111), and (022) Bragg reflections for Cl/Si(113) prepared at 600 °C. The Cl coverage amounts to approximately 1.0 $ML_{Si(113)}$.

meet the requirements for a single adsorption site interpretation (as is generally assumed, e.g., in the case of Cl/Si(111)$-(1\times1)$, where the Cl atoms are almost exclusively adsorbed in on-top sites and typically coherent fractions on the order of $f^{111}\approx0.8$ are determined[25]). However, this simple picture is contradicted by the result for the coherent fraction in (111) geometry, f^{111}=0.53. Therefore, taking into account the results for all reflections hints toward the existence of a highly ordered although more complex adsorbate structure.

Further indication for a common physical building block is gained by characterizing the influence of the Cl surface coverage on the formation and abundance of reconstructions. Figure 4 shows the XSW results obtained for a sample with a Cl uptake of about 1.0 ± 0.2 ML. The LEED pattern (not shown) exhibited a streaky (2×5) pattern. Interestingly, the XSW data seem virtually unchanged with respect to the higher coverage sample (cf. Fig. 3) since all measured coherent fractions and coherent positions differ only by 0.03 at most. These findings manifest the presence of identical atomic subunits within $(2\times n)$-like reconstructions of a *missing row* type.[13]

A further reduction in the Cl coverage by about one order of magnitude was achieved by postannealing the previous sample (Fig. 4) for 150 s at 670 °C, i.e., very close to the desorption temperature of Cl on Si(111), which by temperature-programed desorption was determined to about 680 °C.[26] The corresponding XSW data are depicted in Fig. 5, and again, the coherent fractions and positions remain virtually unchanged. Although merely 0.1 ML of Cl atoms have remained on the surface, and already an incoherent superposition of a faint $(2\times n)$ and a (3×2) periodicity shows up in the respective LEED pattern (not displayed), again the atomic arrangement on the Cl-covered part of the surface has to be very similar to the previous cases. Hence, in the full range of coverages accessible, a set of reconstructions prevails, which all contain the same structural building blocks. Also, the atomic adsorbate structure does not seem to depend on the specific type of preparation: In Fig. 6, XSW data obtained in (113) Bragg geometry are represented after dosing the sample at room temperature and subsequent annealing at 600 °C. For this sample, which exhibited a coverage of about 2 ML, a slightly higher coherent fraction of f^{113}=0.86 for an otherwise unchanged coherent position Φ^{113}=0.88 is obtained. Since this particular experiment has been

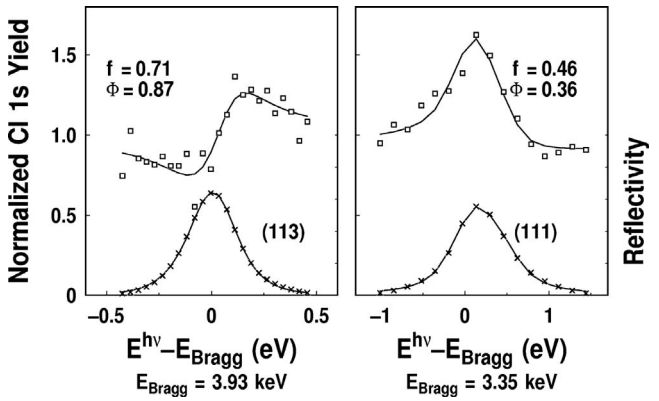

FIG. 5. XSW data and fit (solid lines) for sample reflectivity (×), and Cl 1*s* photoelectron yield (□) in (113) and (111) Bragg reflections for Cl/Si(113), prepared at 600 °C and postannealed at 670 °C. The Cl coverage amounts to approximately 0.1 $ML_{Si(113)}$.

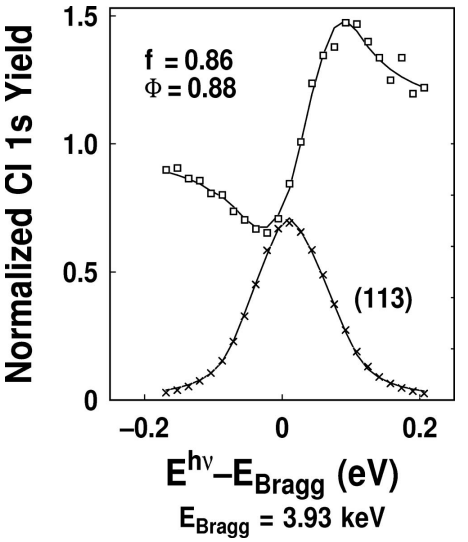

FIG. 6. XSW data and fit (solid lines) for sample reflectivity (×), and Cl 1*s* photoelectron yield (□) in (113) Bragg reflection for Cl/Si(113) saturation dosed at RT and annealed at 600 °C. The Cl coverage amounts to approximately 2.0 $ML_{Si(113)}$.

conducted in a nondispersive XSW setup, we conclude that in our case the measurements of the (113) Fourier components presented above are only marginally affected by the dispersity of the setup employed.

C. Density-functional theory: Calculational details and atomic trial structures

In order to develop structural models for the Cl/Si(113) system, an intuitive approach is to consider the vicinal surfaces of (111) and (001), for which Cl adsorption has been extensively studied in the past.[27] Accordingly, two basic Cl adsorption sites, i.e., the on-top (O) configuration and the symmetric dimer (D) configuration, seem most likely. The resulting $p(2\times1)$ reconstruction is displayed in Fig. 7. For illustration purposes, the atomic Cl rows extending in $[1\bar{1}0]$ direction are denoted according to the bonding configuration as D and O, respectively. This structure and the following structural models have been calculated using *ab initio* DFT within the local-density approximation, and employing a plane-wave basis set as implemented in the program package PWSCF.[28] An electronic high-energy cutoff of 16 Ry and a $2\times2\times1$ set of $\vec{k}$ points were found to be adequate in order to ensure convergence also with special focus on the resulting geometric structure, which poses an additional and sharp criterion in the XSW analysis of DFT-calculated structures.[24] As pseudopotentials, norm-conserving potentials[29,30] have been employed. In the repeated-slab calculations, 12 atomic Si layers have been implemented to account for the relaxation of the uppermost surface layers. During the relaxation, the lowest two Si bilayers have been fixed to ideal bulk coordinates, which also provide the reference layers for the XSW analysis. In order to compare the DFT results to the experimental XSW data, the (111), (113), and (022) Fourier components of the Cl atoms within the relaxed model configurations were calculated. The results for all trial structures considered are listed in Table I along with the experimental data. All calculations were performed with and without a layer of hydrogen atoms at the backside of the slab in order to saturate the dangling bonds. While all structures could be relaxed nicely using both approaches yielding very similar geometries, it was found that hydrogen termination for Si(113) introduces additional strain in the deeper silicon layers, resulting in slightly worse agreement with the experimentally determined Fourier components. In the following, we will restrict the discussion to the results obtained without

TABLE I. Results of the XSW measurements for Cl/Si(113) samples with varying Cl coverage. The theoretical predictions for various structural models are based on DFT structure optimizations (see text for details). The mean deviation δ with respect to the sample with 1.0 ML coverage is listed.

Structure/Coverage	f_c^{113}	Φ_c^{113}	f_c^{111}	Φ_c^{111}	f_c^{022}	Φ_c^{022}	δ
(1.3 ± 0.2) ML	0.75	0.89	0.53	0.39	0.77	0.64	
(1.0 ± 0.2) ML	0.75	0.88	0.54	0.36	0.79	0.63	0.00
0.1 ML	0.71	0.87	0.46	0.36			
$p(2\times1)$ (DO)	0.72	0.08	0.12	0.53	0.93	0.80	0.32
(1×1) (A)	1.00	0.90	1.00	0.42	1.00	0.66	0.20
$p(2\times2)$ (DAO)	0.54	0.04	0.41	0.42	0.70	0.76	0.22
$p(2\times5)$ $[D(A)_4O]$	0.72	0.93	0.71	0.37	0.83	0.67	0.12

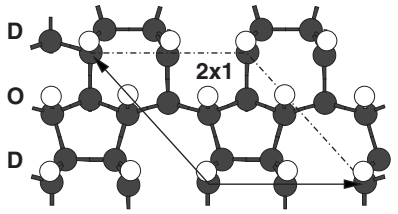

FIG. 7. Top view of a trial $p(2\times1)$ surface reconstruction for Cl/Si(113) as calculated by DFT. Silicon atoms are marked by dark gray and Cl atoms by open circles, respectively. For clarity, only one bulklike Si bilayer is shown. The $p(2\times1)$ surface unit cell is indicated.

hydrogen termination. However, we note that the main conclusions of this paper remain unaffected regardless of the details of the backside termination.

Upon first inspection, the DFT calculations for this $p(2\times1)$ structure (as shown in Fig. 7) yield reasonable results for the Si-Cl bond lengths (2.05 Å $\lesssim d_{\text{Si-Cl}} \lesssim$ 2.07 Å) while the bond length ($d_{\text{Si-Si}}$=2.40 Å) of the Si-Si dimer, which is oriented along the $[1\bar{1}0]$ direction, appears slightly stretched with respect to the Si bulk bond length of 2.34 Å, as determined for the specific Si pseudopotential employed. However, the Fourier components calculated for this trial structure fail to explain the experimental findings for all Bragg reflections, as can readily be seen from $\Phi^{113}_{2\times1}=0.08$, $f^{111}_{2\times1}=0.12$, $\Phi^{111}_{2\times1}=0.53$, and $\Phi^{022}_{2\times1}=0.80$. Although this structural model may seem quite intuitive on first glance, it neither reproduces the XSW-derived Fourier components nor does it account for the $p(2\times2)$ periodicity observed in LEED. Hence, additional Cl adsorption geometries have to be investigated.

As a second attempt we consider the (1×1)-reconstructed Cl/Si(113) surface with a surface unit cell composed of a single Cl atom adsorbed on top of a Si adatom (this configuration is labeled "A" in the following), as displayed in Fig. 8. Naturally, all calculated coherent fractions are equal to unity if perfect ordering is assumed. An analysis of the bond lengths in the near-surface region reveals that only the Si-Cl bond exhibits a reasonable value of $d_{\text{Si-Cl}}$=2.07 Å while the Si-Si backbonds, i.e., the bonds of the Si adatom to its three nearest Si neighbors, appear severely elongated ($d_{\text{Si-Si}}$ =2.41 Å and $d_{\text{Si-Si}}$=2.69 Å, respectively). Nevertheless, the XSW calculation reveals a very good agreement with the

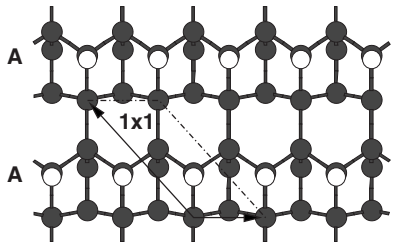

FIG. 8. Top view of a trial (1×1) surface reconstruction for Cl/Si(113) as calculated by DFT. Silicon atoms are marked by dark gray and Cl atoms by open circles, respectively. For clarity, only one bulklike Si bilayer is shown. The (1×1) surface unit cell is indicated.

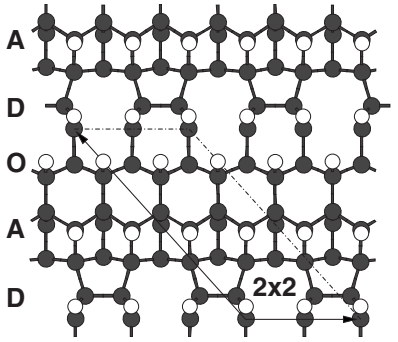

FIG. 9. Top view of a trial $p(2\times2)$ surface reconstruction for Cl/Si(113) as calculated by DFT. Silicon atoms are marked by dark gray and Cl atoms by open circles, respectively. For clarity, only one bulklike Si bilayer is shown. The $p(2\times2)$ surface unit cell is indicated.

experimental data (given in brackets for comparison) for the coherent positions, which amount to $\Phi^{113}_{1\times1}=0.90(0.89)$, $\Phi^{111}_{1\times1}=0.42(0.39)$, and $\Phi^{022}_{1\times1}=0.66(0.64)$. However, as no (1×1) LEED pattern has been observed for the whole range of Cl coverages investigated, we interpret these results in the sense that the Cl bonding geometry on top of a Si adatom is a probable and frequent structural building block of the Cl/Si(113) surface structure.

Based on the results of the preceding paragraphs, a logical extension of the $p(2\times1)$ structure to a $p(2\times2)$ reconstruction is close at hand by inserting an additional row of adatoms in $[1\bar{1}0]$ direction, as depicted in Fig. 9.

In comparison to the $p(2\times1)$ structure, which in our case we denote as the dimer-*on top* (DO) model in the following, the dimer-adatom-*on top* (DAO) model exhibits only a slightly stretched Si-Si dimer bond length of $d_{\text{Si-Si}}$=2.43 Å. All the other Si-Si bonds in the near-surface region, and especially the backbonds of the Si adatom, are significantly relaxed with respect to the (1×1) structure [adatom (A) model in our nomenclature]. For specific bonds that are mainly oriented along the $[33\bar{2}]$ direction, this bond-length contraction amounts up to −0.23 Å, indicating substantial strain release. This is actually confirmed from the calculation of the stress tensor elements σ_{yy} ($\hat{y}\|[33\bar{2}]$) for both structural models that prove a stress release of about 25% for the DAO model with respect to the A model.

Turning now to the XSW analysis of the DAO model, the Fourier components were determined to be $f^{113}_{2\times2}=0.54$, $\Phi^{113}_{2\times2}=0.04$, $f^{111}_{2\times2}=0.41$, $\Phi^{111}_{2\times2}=0.42$, $f^{022}_{2\times2}=0.70$, and $\Phi^{022}_{2\times2}=0.76$. Consequently, the agreement between the experimental and the calculated data has considerably improved, as compared to the $p(2\times1)$ model. As a larger contribution of adatom sites significantly decreases the discrepancy between the experimental data and the theoretical result, the DAO model may be extended in the following way: By inserting an additional Cl adatom row such that the model may be denoted as DAAO, a (2×3) surface structure may be constructed. Upon repetition of this procedure, arbitrary $(2\times n)$ reconstructions denoted as $\text{D(A)}_{n-1}\text{O}$ may be built, exhibiting ideal Cl coverages equal to $(n+1)/n$ ML. This way of increasing the adatom coverage is endorsed by the fact that

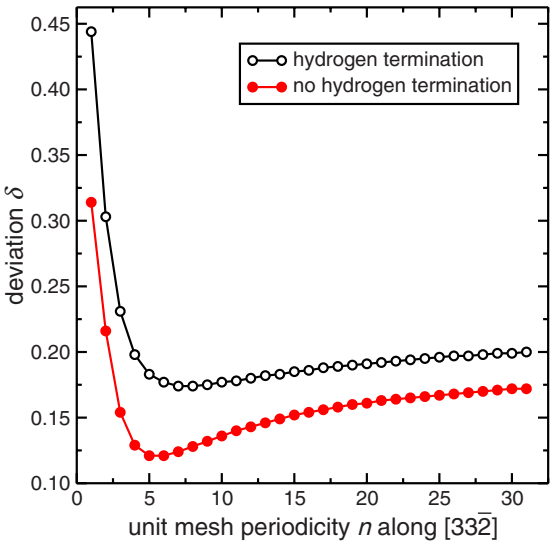

FIG. 10. (Color online) Variation of mean deviation δ depending on $(2\times n)$ reconstruction within the $D(A)_{(n-1)}O$ model for the experimental XSW data set determined for a Cl coverage of 1 ML, calculated from DFT-derived Fourier components with and without hydrogen termination on the backside of the slab.

the STM images[13] and the LEED patterns (almost) always showed a complex $(2\times n)$ surface structure. A thorough theoretical treatment of this large variety of $D(A)_{n-1}O$ structures would require fully independent DFT calculations for all trial structures including possible defect geometries, which in turn would result in immense computational costs and consequently are beyond the scope of this paper. However, satisfactory results may already be gained by approximating the Fourier components of the general $D(A)_{n-1}O$ model as the normalized sum of the DAO Fourier components and $(n-2)$ Fourier components of the simplified (1×1) adatom model. Hence, all (hkl) Fourier components of the individual $D(A)_{n-1}O$ structure solely depend on n, allowing an average value of n to be determined for a given set of experimental XSW data in a simple least-square fitting routine. This is illustrated in Table I by the average deviation δ of the calculated Fourier components from the measured Fourier components (as defined by their root-mean-square in the complex plane), which is given for a fit to the experimental data shown in Fig. 4 (1 ML Cl coverage). Accordingly, a best fit is obtained for $n\approx 5$, i.e., a $D(A)_4O$ model (see Fig. 10): $f_{2\times5}^{113}=0.72$, $\Phi_{2\times5}^{113}=0.93$, $f_{2\times5}^{111}=0.71$, $\Phi_{2\times5}^{111}=0.37$, $f_{2\times5}^{022}=0.83$, and $\Phi_{2\times5}^{022}=0.67$. For this (2×5) structure, a theoretical Cl coverage of 1.2 ML is calculated, which is in good agreement with the experimental result of about 1 ML (see Table I). Of course, in reality one should expect coexistence of several $(2\times n)$ phases with different "local" n, implying that the calculated value n should be considered its large-scale average. This interpretation would lead to the presence of nanoscale regions of varying Cl coverage, as has already been observed in STM.[13]

D. Adsorption at room temperature

Analogous to the theoretical simulation of the adsorption of H on Si(113)-(3×2),[11] we expect the pentamer structure

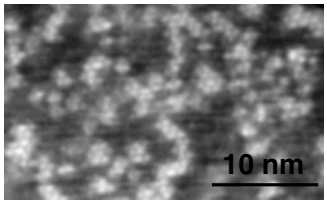

FIG. 11. STM image ($U_{tip}=1.0$ V and $I=0.3$ nA) recorded after exposure to Cl_2 at room temperature, exhibiting areas (bright) of local (2×2) periodicity.

of the (3×2) reconstructed clean Si surface, and especially the interstitial sixfold coordinated Si atom, to be energetically unstable upon Cl_2 exposure. Thus, after dissociation of impinging Cl_2 molecules and removal of the interstitial Si from its original site, the surface will offer a variety of dangling bonds that may be saturated by Cl atoms, possibly inducing the local formation of (2×2)-reconstructed areas. Indeed, compelling evidence for such a process is presented in Fig. 11, which shows a STM image taken from a surface area with a particularly high density of reacted sites. The corresponding LEED pattern exhibits a diffuse (3×2) periodicity, which proves that the underlying substrate reconstruction has not been lifted completely on a larger scale.

Eventually, annealing at 600 °C induces a substantial surface mobility of the Cl and the Si atoms, which enables the reconstruction of the surface layers. Since the number of Si atoms missing in order to create a (2×2) reconstruction in the DAO model averages 2.5 atoms per unit cell, these Si atoms are likely to be supplied by step edges that, after annealing, have been shown to exhibit long and straight sections with outward normals pointing along the $[33\bar{2}]$ direction.[13] Hence, the formation of the adatom rows and the conversion of the formerly (3×2) reconstructed surface areas to a local $(2\times n)$ structure are intimately related to the straightening and alignment of the step edges with respect to the adatom rows.

E. Implications for step-edge geometries on vicinal surfaces

The findings for Cl on Si(113) as presented in the previous paragraphs have far-reaching consequences also for the halogen-terminated stepped Si(111) and Si(001) surfaces since the chlorinated Si(113) surface may alternatively be viewed as a maximally stepped Si(111) and Si(001) surface, respectively (Fig. 12).

For Si(111), the bilayer step edges exhibit outward normals in $\langle\bar{1}\bar{1}2\rangle$ direction that, using STM, we found as the only orientation occurring for Cl adsorption on Si(111) at

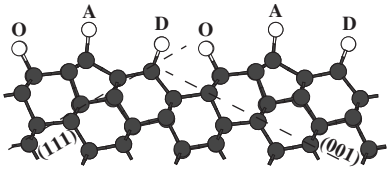

FIG. 12. Side view of the DAO model for Cl/Si(113) as determined from DFT. Silicon atoms are marked by dark gray and Cl atoms by open circles, respectively. (001) and (111) oriented crystal planes are indicated.

elevated temperatures or subsequent annealing, in accordance with the literature.[31] An atomic model of this so-called *A*-type step-edge geometry has already been proposed based on STM investigations for Br/Si(111) (Ref. 31) and H/Si(111).[32] Our DFT calculations for this certain kind of step-edge structure predict atomic coherent positions of the Cl step-edge atoms of $\Phi_{\text{step}}^{113}=0.90$, $\Phi_{\text{step}}^{111}=0.34$, and $\Phi_{\text{step}}^{022}=0.63$, which are in very good agreement with the Fourier components of the A model for Cl/Si(113). Thus, our findings for the chlorinated Si(113) surface, which clearly demonstrate the prevalence of Cl adatom sites, strongly suggest that the local atomic configuration of the Si(111) step edges decorated by Cl atoms is virtually identical to the previously introduced Cl adatom site on the Si(113) surface.

For Si(001), it is readily conceived that the local bonding geometry of the adatom site on Si(113) is identical to the reconstructed *B*-oriented double-layer (D_B) step-edge structure as introduced by Chadi for the bare Si(001) substrate (Fig. 12).[33] In fact, this particular step-edge structure was calculated to be the stable configuration for double-layer steps as opposed to the nonreconstructed variant. Hence, in the case of Si(001), it is apparent that this feature of the bare substrate is preserved in the presence of halogen adsorbates. Based on these findings regarding the Si(001), Si(111), and Si(113) surfaces, we propose that all halogenated Si(11*n*) surfaces are generally made up of essentially the same atomic building blocks, i.e., dimer, adatom, and on-top sites. Thus, their relative coverage will be determined by the specific choice of miscut angle.

IV. CONCLUSION

We have studied the interaction of Cl with the clean Si(113) surface under UHV conditions by a variety of experimental surface science techniques and theoretical calculations. Upon Cl adsorption, the original (3×2) reconstruction is lifted and replaced by a patchwork of local $(2\times n)$ reconstructions of varying Cl content but similar structural subunits. Using a combination of XSW and DFT, we propose the following structure for the fundamental $p(2\times2)$ reconstruction: Cl atoms at Si dimer sites, Cl atoms bonding on top of Si adatoms, and Cl atoms located (almost) *on top* of one-fold unsaturated Si substrate atoms. In this DAO model consisting of alternating atomic rows of each component along the $[1\bar{1}0]$ direction, the A adsorption site is the key structural element, which enables the formation of a whole set of DAO-like $(2\times n)$ surface reconstructions by repeated insertion of $(n-2)$ additional Cl adatom site rows ($DA_{n-1}O$ structure). Interestingly, the observed prevalence of the Cl adatom site on Si(113) allows us to also settle the issue of the atomic step-edge structure for halogen-terminated Si(111) surfaces. Our DFT calculations and subsequent XSW simulations reveal the obvious analogy of the adatom site and the *A*-type step-edge geometry, strongly suggesting that these step-edge sites are sequentially populated for increasingly vicinal Si(111) surfaces approaching the (113) orientation. Likewise, the results presented here corroborate the stability of reconstructed D_B-type step edges for halogenated vicinal Si(001) surfaces, suggesting that the relative surface coverage of the majority adsorption sites, i.e., dimer, adatom, and on-top sites, can be tuned by choosing an appropriate miscut angle.

ACKNOWLEDGMENTS

The authors would like to thank Mehmet Çakmak for helpful suggestions and discussions as well as the authors of the package PWSCF (Ref. 28).

*flege@ifp.uni-bremen.de

[1] H.-J. Müssig, J. Dąbrowski, K.-E. Ehwald, P. Gasworzewski, A. Huber, and U. Lambert, Microelectron. Eng. **56**, 195 (2001).
[2] H. Omi and T. Ogino, Appl. Phys. Lett. **71**, 2163 (1997).
[3] M. P. Halsall, H. Omi, and T. Ogino, Appl. Phys. Lett. **81**, 2448 (2002).
[4] Z. Zhang, K. Sumitomo, H. Omi, T. Ogino, J. Nakamura, and A. Natori, Phys. Rev. Lett. **88**, 256101 (2002).
[5] H. Suzuki, H. Nakahara, S. Miyata, and A. Ichimiya, Surf. Sci. **493**, 166 (2001).
[6] T. Clausen, Th. Schmidt, J. I. Flege, A. Locatelli, S. Heun, T. O. Mentes, F. Guo, and J. Falta, e-J. Surf. Sci. Nanotechnol. **3**, 379 (2005).
[7] Th. Schmidt, T. Clausen, J. I. Flege, S. Gangopadhyay, A. Locatelli, T. O. Mentes, F. Z. Guo, S. Heun, and J. Falta, New J. Phys. **9**, 392 (2007).
[8] U. Myler and K. Jacobi, Surf. Sci. **220**, 353 (1989).
[9] W. Ranke, Phys. Rev. B **41**, 5243 (1990).
[10] J. Dąbrowski, H. J. Müssig, and G. Wolff, Phys. Rev. Lett. **73**, 1660 (1994).
[11] J. Dąbrowski, H.-J. Müssig, and G. Wolff, J. Vac. Sci. Technol. B **13**, 1597 (1995).
[12] H. F. Winters and J. W. Coburn, Surf. Sci. Rep. **14**, 162 (1992), and references therein.
[13] J. I. Flege, Th. Schmidt, G. Materlik, and J. Falta, Surf. Sci. **566-568**, 94 (2004).
[14] J. I. Flege, Th. Schmidt, J. Bätjer, M. Çakmak, G. Materlik, and J. Falta, New J. Phys. **7**, 208 (2005).
[15] B. W. Batterman and H. Cole, Rev. Mod. Phys. **36**, 681 (1964).
[16] J. Zegenhagen, G. Materlik, and W. Uelhoff, J. X-Ray Sci. Technol. **2**, 214 (1990).
[17] I. A. Vartanyants and J. Zegenhagen, Solid State Commun. **113**, 299 (1999).
[18] F. Tamarit and C. Anteneodo, Phys. Rev. Lett. **84**, 208 (2000).
[19] F. Schreiber, K. A. Ritley, I. A. Vartanyants, H. Dosch, J. Zegenhagen, and B. C. C. Cowie, Surf. Sci. **486**, L519 (2001).
[20] J. Stanzel, W. Weigand, L. Kilian, H. L. Meyerheim, C. Kumpf, and E. Umbach, Surf. Sci. **571**, L311 (2004).
[21] K. Kern and D. A. Poutinen, RCA Rev. **31**, 187 (1970).
[22] N. D. Spencer, P. J. Goddard, P. W. Davies, M. Kitson, and R. M. Lambert, J. Vac. Sci. Technol. A **1**, 1554 (1983).

[23] A. Szabó, P. D. Farrall, and T. Engel, Surf. Sci. **312**, 284 (1994).
[24] M. Siebert, Th. Schmidt, J. I. Flege, and J. Falta, Phys. Rev. B **72**, 045323 (2005).
[25] J. I. Flege, Th. Schmidt, J. Falta, and G. Materlik, Surf. Sci. **507-510**, 381 (2002).
[26] P. Gupta, P. A. Coon, B. G. Koehler, and S. M. George, Surf. Sci. **249**, 92 (1991).
[27] C. M. Aldao and J. H. Weaver, Prog. Surf. Sci. **68**, 189 (2001).
[28] S. Baroni, A. D. Corso, S. de Gironcoli, and P. Giannozzi, The PWSCF (plane-wave self-consistent field) package, http://www.pwscf.org
[29] G. B. Bachelet and M. Schlüter, Phys. Rev. B **28**, 2302 (1983).
[30] X. Gonze, R. Stumpf, and M. Scheffler, Phys. Rev. B **44**, 8503 (1991).
[31] B. S. Itchkawitz, M. T. McEllistrem, and J. J. Boland, Phys. Rev. Lett. **78**, 98 (1997).
[32] F. Owman and P. Mårtensson, Surf. Sci. **324**, 211 (1995).
[33] D. J. Chadi, Phys. Rev. Lett. **59**, 1691 (1987).